Trajectory Planning for a 3-SPS-U Tensegrity Mechanism

Swaminath Venkateswaran, Damien Chablat

Proceedings of the ASME 2021 International Design Engineering Technical Conferences & Computers and Information in Engineering Conference
IDETC/CIE 2021
August 17–20, 2021, Virtual, Online

DETC2021/MR69957

TRAJECTORY PLANNING FOR A 3-SPS-U TENSEGRITY MECHANISM

Swaminath Venkateswaran
G-SCOP Laboratory
Grenoble Institute of Technology
46 Avenue Félix Viallet, 38031 Grenoble, France
Email: swaminath.venkateswaran@grenoble-inp.fr

Damien Chablat*
Centre National de la Recherche Scientifique (CNRS)
Laboratoire des Sciences du Numérique de Nantes (LS2N)
UMR CNRS 6004, 44321 Nantes, France
Email: damien.chablat@cnrs.fr

ABSTRACT

This article presents the actuation strategy of a 2-DOF tensegrity type mechanism that employs three tension springs and a passive universal joint. This mechanism is proposed to be incorporated as an articulation unit for a piping inspection robot in order to overcome pipe bends and junctions. In the event of a junction, external actuations are required to allow the mechanism as well as the robot to follow a certain direction. Using DC-motors coupled with encoders, experiments are carried out on a test bench of the tensegrity mechanism. The actuation of the mobile platform is performed using cables that pass through each spring. By correlating the architecture to a 3-SPS-U parallel mechanism, the singularity-free workspace of the mechanism is analyzed to identify the tilt limits. A closed-loop PID controller is implemented using a microcomputer to perform a linear trajectory within the singularity-free workspace. The Inverse Kinematic Problem (IKP) is solved by passing input tilt angles to the controller. With the help of a force control algorithm, the experiments are carried out under no-load conditions for vertical and horizontal orientations of the mechanism. The error data of the joint positions and the motor torques are then interpreted for both orientations of the mechanism.

INTRODUCTION

Tensegrity structures are deployable mechanisms that comprise strings in tension and bars in compression [1]. Tensegrity structures have created a major attention in the field of civil engineering [2] and robotics [3–5]. The Snelson's X-shape planar tensegrity mechanism is a well-known architecture studied by the scientific research community [6, 7]. However, the analysis on this model is limited to 2D configuration [8]. As a part of research project with AREVA, a rigid bio-inspired caterpillar type piping inspection robot was designed and developed at LS2N, France [9]. Through the study of design issues associated with pipelines, a tensegrity mechanism that employs three tension springs and a passive universal joint was incorporated into this robot to have a flexible design [10]. The mechanism can operate in a 3D workspace under passive modes for a 90° pipe bend and in the event of a junction, cable actuation can be performed to follow a given path. This article focuses on the actuation strategy of the tensegrity mechanism, which corresponds to addressing the issue of active compliance [10]. The actuation strategy of the mechanism is similar to that of a parallel manipulator. Parallel kinematics machines (PKM) have interesting applications in the industries over serial machines. PKM's offer better accuracy, lower mass/inertia properties and high structural stiffness [11]. The performance of parallel robots varies within their workspace, which is considerably smaller when compared to serial robots. The inverse kinematics, in general, is easier to solve for parallel robots, especially when prismatic joints are employed. The 3-SPS-U architecture employs three actuated prismatic springs and the IKP appears simpler. However, it is complicated to determine the inverse of the Jacobian matrices for parallel robots and the computation times appear to be higher. For the tensegrity mechanism, the Jacobian matrix can be obtained from the direct kinematics matrix. The simpler architecture of the mechanism

*Address all correspondence to this author.

makes it easier to identify the cartesian velocities and accelerations. The most important step will be to plan a trajectory in such a way that the mechanism operates within the singularity-free workspace. In the initial step, the workspaces are verified numerically for the prototype of a 3-SPS-U tensegrity mechanism using the CAD algorithm. This analysis provides the tilt and the joint limits for the mechanism within the singularity-free workspace. By using these limits, experiments are conducted on the prototype using DC-motors. The DC-motors are equipped with position encoders which gives information about each angular displacement of the output shaft. Two algorithms were studied in [12] viz: Force control and Position control algorithms. The former is employed in the experiments to control the tilt limits of the mechanism. By providing the tilt angles as inputs, the position, velocity and acceleration of each prismatic joint are controlled. For attaining the desired position for a given tilt angle, a simplified Proportional-Integral-Derivative (PID) algorithm is employed. A BeagleBone(BB) black microcomputer is used to accomplish this closed-loop system. A linear trajectory is performed on the tensegrity mechanism for vertical and horizontal orientations. By performing experiments on the prototype, the actual position, the motor torques and the error between the measured and desired data are represented and studied. The experiments carried out on the prototype will set up a foundation for the mechanism actuation when it is coupled along with the piping inspection robot in order to follow a certain direction while encountering a junction.

The outline of the article is as follows. Initially, the geometric equations and the workspace analysis of the tensegrity mechanism are presented. Followed by that, the experimental setup and interfacing with the controllers are discussed. The subsequent section presents the trajectory planning and algorithm employed in the control law. Then, the results of experiments are presented. The article then ends with discussions and conclusions.

ARCHITECTURE AND WORKSPACE OF THE MECHANISM

This section presents the architecture of the tensegrity mechanism and its associated constraint equations. The workspace of the mechanism is also presented which will be then employed to carry out experiments.

Geometrical equations

The tensegrity mechanism comprises a base and an end-effector which are coupled together by three tension springs and a passive universal joint. For exploiting the geometric equations, the mechanism is correlated to a parallel manipulator of type 3-SPS-U. The architecture of the mechanism at the home-pose where the tilt angles η and ϕ are zero is represented in Fig. 1. The fixed coordinate frame of the base is represented by $\sum_0$ with its origin at B_0. The spring mounting points on the fixed base are represented by B_1, B_2, B_3 and they form the imaginary equilateral triangle of the manipulator base. The vector coordinates for the base mounting points can be written as:

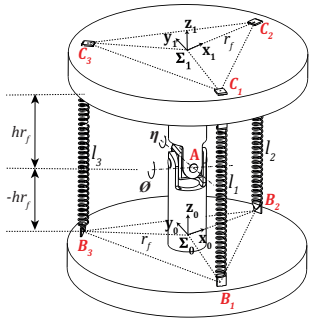

FIGURE 1. 3D model of the 3-SPS-U tensegrity mechanism at the home-pose

$$\mathbf{b}_{i+1} = \left[r_f \cos\left(\frac{i2\pi}{3}\right), r_f \sin\left(\frac{i2\pi}{3}\right), -r_f h \right]^T, \text{with } i = 0,1,2 \tag{1}$$

In Eqn. (1), h is a constant which determines the static stability of the mechanism [10]. For studying the singularity-free workspace of the mechanism, the Euler-angles of the universal joint are employed to identify the constraint equations of the end-effector whose coordinates are given by:

$$\mathbf{c}_{i+1} = \mathbf{R}_x(\eta)\mathbf{R}_y(\phi) \left[r_f \cos\left(\frac{i2\pi}{j}\right), r_f \sin\left(\frac{i2\pi}{j}\right), r_f h \right]^T \tag{2}$$

with $i = 0,1,2$

The IKP which determines the length of the prismatic springs is computed by calculating the distance between base and end-effector at the home-pose and working conditions. The equation is given by:

$$l_i = \sqrt{(b_{ix} - c_{ix})^2 + (b_{iy} - c_{iy})^2 + (b_{iz} - c_{iz})^2}\ , i = 1 \text{ to } 3 \tag{3}$$

It has to be noted that the mechanism has 2 degrees of freedom. At any instant, only one cable actuation or two cable actuations are required to tilt the mobile platform. This proves the redundancy of the mechanism. When the mechanism is coupled with the piping inspection robot, during locomotion, the information about the pipe bend and profile is unknown. Based on the profile encountered, either one or two of the three springs are actuated to tilt along a given direction. Also, the presence of a redundant third spring ensures the static stability of the mechanism.

Workspace analysis

For identifying feasible workspaces for the mechanism, it is important to study the singularities. For a parallel mechanism, the singularity equation is given by the well-known equation [13]:

$$\mathbf{A}\mathbf{t} + \mathbf{B}\dot{\rho} = 0 \tag{4}$$

where $\mathbf{t}$ represents the angular velocity vector and $\dot{\rho} = [\dot{l_1}, \dot{l_2}, \dot{l_3}]^T$ represents the joint velocity vector.

In Eqn. (4), $\mathbf{A}$ represents the direct-kinematics matrix or forward Jacobian matrix and $\mathbf{B}$ represents the inverse-kinematics matrix or inverse Jacobian matrix of the mechanism. The pose variables for the mechanism are the tilt angles η and ϕ. The articular variables are the lengths: l_1, l_2 and l_3. For the tensegrity mechanism, the three types of singularities namely Type-1, Type-2 and Type-3 [13–15] are verified using Eq. (4). From the number of pose variables and articular variables, it could be seen that the matrix $\mathbf{A}$ does not correspond to a $n \times n$ square matrix. For identifying the singularity equations and to construct a square matrix, the 3-SPS-U mechanism is split into three sets of 2-SPS-U architecture which comprises of length pairs $l_1 - l_2$, $l_2 - l_3$ and $l_1 - l_3$ [16]. It was studied in [16] that there exists no serial singularities in the mechanism for a mechanism with r_f = 11 mm and h=1. This configuration is scaled up to carry out experiments on the tensegrity mechanism where r_f is taken as 56.7 mm. A stability analysis carried out in [17] is verified for the 3-SPS-U mechanism and the value of h is chosen as 0.6. By setting joint limits, the singularity-free workspace is extracted for the tensegrity mechanism by using the CAD algorithm in Maple [16]. A linear trajectory is chosen within the singularity-free workspace square bounded by $\pm 2\pi/15$ radians to perform experiments on the prototype.

EXPERIMENTAL SETUP

Using tensions springs, universal joint and platforms realized by rapid prototyping, the 3-SPS-U tensegrity mechanism is assembled. The control of the mechanism is carried out using a BB black [12] micro-computer. In order to have a higher torque, a static model is validated by the actuation of the springs through a DC-motor coupled with a planetary gearhead. In general, a DC motor speed control can be achieved through variation of voltage but the position control of the motor shaft is difficult to achieve [18]. The DC motors are integrated with quadrature encoders which provides information about the motor pulse counts for every revolution of the output shaft of the gearbox. The direction control of DC motors is achieved using microcontrollers that use an H-bridge module, which is controlled through PWM duty cycles from BB black. In order to attain the desired prismatic length and tilt the tensegrity mechanism, a simplified Proportional-Integral-Derivative (PID) algorithm is employed to have a closed-loop system. The three DC-motors are assembled on a test bench, which is made by rapid prototyping. The experiments are carried out for two orientations: vertical and horizontal under no-load conditions. The experimental setup in the vertical orientation is represented in Fig. 2.

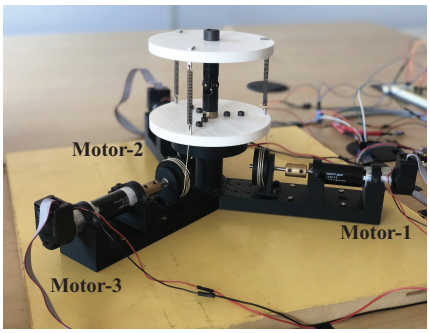

FIGURE 2. Representation of the experimental setup of the tensegrity mechanism in the vertical orientation

Interfacing between mechanism and control units

The actuation of springs is carried out using three Maxon DC-motors (Series-352994) [19]. Each DC-motor has a Maxon 36/2 servo controller for position control. The DC-motors are coupled with a planetary gearhead (Series-144041) which has a reduction ratio of 1621:1. Thus, higher output torque is obtained at the gearbox output shaft. Quadrature encoders are integrated with each DC-Motor. The supply voltage for the encoders is 5 V and they can read 500 counts for every change in the angular position of the DC-motor. For controlling the DC motor direction and input power supply, the PWM and GPIO pins of BB black are employed. As, the maximum voltage supported by these pins is 3.3 V, a 1 kΩ potential divider bridge is employed to step down the voltage from the encoder output pins.

TRAJECTORY PLANNING AND CONTROL STRATEGY

In the experimental validation, the IKP is solved. This means that a set of tilt angles η and ϕ are passed as inputs to the control loop and the IKP is solved through actuation of the motors connected to the springs. The pose variables and the articular variables for the mechanism are given by $\mathbf{q} = [\eta, \phi]$ and $\rho = [l_1, l_2, l_3]$. The length of each spring for a given tilt angle can be estimated using Eqn. (3). The IKP for each spring is converted into angular displacements of the pulley, which will be the target position for each DC-motor. The equation for the desired angular

position of the pulley with respect to the IKP is given by:

$$\theta_{di} = \frac{(l_i - l_{home})}{r} \text{ , with } i = 1,2,3 \tag{5}$$

In Eqn. (5), θ_{di} is the desired angular position calculated from IKP for given input tilt angles η and ϕ. The parameter r indicates the pulley radius, which is 20 mm. At the home position, the value of l_{home} is 68 mm for r_f = 56.7 mm and h= 0.6. For every angular displacement of the DC-motor, encoder data is passed to the BB black ports. The angular displacement of the pulley from the encoder channel information can be calculated by:

$$\theta_{mi} = \frac{E_i \pi}{2CG} \text{ , with } i = 1,2,3 \tag{6}$$

In Eqn. (6), E_i indicates the output data of the encoder channels of Motor-i. The angle θ_{mi} is the measured angular displacement at the output shaft of the gearbox. C indicates the counts per revolution of the encoder and G is the reduction ratio of the gearbox. At a given tilt angle, the mechanism tries to attain the position θ_{di}. In order to minimize the errors between the desired and measured angular positions, the PID control algorithm is employed.

Trajectory generation

The trajectory planning approach proposed in [20] is employed for the control of the tensegrity mechanism. For every angular displacement of the DC-Motor, it is necessary to determine the joint velocities and accelerations for the mechanism. During the change of tilt angles from home-pose to the desired position, the Cartesian velocities of the prismatic joints can be calculated using Eqn. (7) [21].

$$\begin{bmatrix} \dot{l_1} \\ \dot{l_2} \\ \dot{l_3} \end{bmatrix} = \mathbf{J}_c \begin{bmatrix} \dot{\eta} \\ \dot{\phi} \end{bmatrix} \text{ , with } \mathbf{J}_c = \begin{bmatrix} \frac{\partial l_1}{\partial \eta} & \frac{\partial l_1}{\partial \phi} \\ \frac{\partial l_2}{\partial \eta} & \frac{\partial l_2}{\partial \phi} \\ \frac{\partial l_3}{\partial \eta} & \frac{\partial l_3}{\partial \phi} \end{bmatrix} \tag{7}$$

In Eqn. (7), $\mathbf{J}_c$ represents the direct kinematics matrix ($\mathbf{A}$) of the tensegrity mechanism. Using Eqn. (7), the joint velocities are estimated, followed by which the desired angular velocities of the output shaft can be estimated. For given input tilt angles, the trajectory generation is carried out using a fifth-degree polynomial equation [20]. This equation is used to define the position $s(t)$, velocity $\dot{s}(t)$ and acceleration $\ddot{s}(t)$ for the mechanism and they are given by:

$$s(t) = P(t) \text{ , } \dot{s}(t) = \frac{\mathrm{d}s(t)}{\mathrm{d}t} \text{ , } \ddot{s}(t) = \frac{\mathrm{d}^2 s(t)}{\mathrm{d}t^2} \tag{8}$$
$$\text{where } P(t) = 10\left(\frac{t}{t_f}\right)^3 - 15\left(\frac{t}{t_f}\right)^4 + 6\left(\frac{t}{t_f}\right)^5$$

For the experiments, a linear trajectory is performed on the tensegrity mechanism for both orientations. The position, velocity and acceleration equations, as well as the maximum simulation time, varies according to the type of trajectory. Initially, minimum travelling time t_f is determined when the velocities and accelerations reach the saturation point in the trajectory. For the fifth degree polynomial, the value of t_f for a linear trajectory is given by [20]:

$$t_f = \max\left(\frac{15|D|}{8k_v}, \sqrt{\frac{10|D|}{\sqrt{3}k_a}}\right) \tag{9}$$

In Eqn. (9), $|D|$ represents the norm of the position, k_v represents the maximum velocity and k_a represents the maximum acceleration. At home-position, let $\mathbf{D}_1$ be the vector that contains the initial tilt angles η_i and ϕ_i. The final tilt positions are given by the vector $\mathbf{D}_2$. The intermediate pose $\mathbf{D}$ is given by:

$$\mathbf{D}(t) = \mathbf{D}_1 + (\mathbf{D}_2 - \mathbf{D}_1)s(t) \tag{10}$$

The corresponding velocity and acceleration vectors can be found using the first and second order derivative of Eqn. (10) with respect to time. The equations are given by [21]:

$$\mathbf{V}(t) = (\mathbf{D}_2 - \mathbf{D}_1)\dot{s}(t) \tag{11}$$
$$\mathbf{A}(t) = (\mathbf{D}_2 - \mathbf{D}_1)\ddot{s}(t) \tag{12}$$

The joint coordinate vector can be obtained by the equation:

$$\mathbf{q}(t) = \mathbf{f}\left(\mathbf{D}(t)\right) \tag{13}$$

In Eqn. (13), $\mathbf{f} = [l_1, l_2, l_3]^T$ is the vector that contains the solution of the IKP for given tilt angles. The joint velocities can be computed with the help of the Jacobian matrix $\mathbf{J}_c$ using the equation:

$$\dot{\mathbf{q}}(t) = \mathbf{J}_c \mathbf{V}(t) \tag{14}$$

The accelerations in the joints can be computed using the Jacobian matrix and it's time derivative. The equation is given by:

$$\ddot{\mathbf{q}}(t) = \mathbf{J}_c\mathbf{A}(t) + \dot{\mathbf{J}}_c\mathbf{V}(t) \tag{15}$$

The desired position, velocity and acceleration vectors of the joints from Eqn. (13) to Eqn. (15) will be used as inputs for the PID algorithm to perform a linear trajectory.

Force control algorithm

A force control algorithm is employed to reach the desired positions for input tilt angles. By applying motor torques and current, the mechanism tilts to attain the desired position. Once the desired position is reached, the current and torque are cut off for attaining a static phase. For each angular position of DC-Motor, encoder position data is transmitted to the user by the BB black. However, the output data from encoders are not directly used to calculate the solutions to the IKP as there exists a significant difference between the desired and measured positions. These differences are caused by factors such as motor inertia, frictional effects and inertial forces. In order to compensate these factors, a closed loop feedback system is employed which tries to minimize the errors between the desired and measured positions. The classical relation for the PID control scheme which provides the motor torque is given by the equation [21, 22]:

$$\begin{aligned}\Gamma = J(\ddot{\theta}_i + K_P(\theta_{di} - \theta_{mi}) + K_D(\dot{\theta}_{di} - \dot{\theta}_{mi}) \\ + K_I \int_0^t (\theta_{di} - \theta_{mi})) \text{ , with } i = 1,2,3\end{aligned} \tag{16}$$

In Eqn. (16), Γ is the regulated torque obtained at the gearbox output shaft after PID correction. For computing the torques induced on each motor, Eqn. (16) is multiplied by the gear reduction ratio G. The inertia of motor-gearbox assembly J is taken as $4.1e-7$ kg.m^2 [19]. The values for the PID terms of Eqn. (16) are given by:

$$\begin{aligned}&\omega = \frac{k_t k_e}{RJ} = 14 \ rad/s \\ &K_P = 3\omega^2 = 588 \ , \ K_D = 3\omega = 42 \ , \ K_I = \omega^3 = 2744\end{aligned} \tag{17}$$

In Eqn. (17), ω is a parameter which is determined from the torque constant (k_t), speed constant (k_e), resistance (R) and inertial parameters (J) of the DC-Motor [21]. Before the start of experiments, the ESCON servo controllers are calibrated in a computer. The saturation current is used as reference for controlling the direction of rotation of the DC-Motors. For safer operations, 90% and 10% duty cycles are set as limits for the rotation of motors on either direction. At these duty cycles, the motors tend to operate at their nominal rating torque of 6.05 mN.m. The force control algorithm is written in C-language to control the tilting of the tensegrity mechanism as well as to attain the desired trajectory using the BB black microcomputer.

RESULTS OF EXPERIMENTS

The experiments are performed for linear trajectory in vertical and horizontal orientations of the mechanism. The vertical orientation is the natural pose of the mechanism as depicted in Fig. 2. This orientation is also inline with the vertical orientation of the bio-inspired robot studied in [9]. The horizontal orientation is the posture when the tensegrity mechanism is coupled with the bio-inspired robot and the assembly is moving inside a horizontal pipeline. Two kinds of experiments are performed for the linear trajectory. In the first experiment, which is called the One spring pull, one of the three springs pulls the end-effector platform. In the second experiment, which is called the Two springs pull, two of the three springs pulls the end-effector platform. While encountering a 90° bend in a junction, one of these two types of linear trajectory actuation can be performed on the tensegrity mechanism so that the inspection robot can follow a certain direction. Due to the memory issues associated with the BB black, both experiments could not be carried out on a single stretch. Firstly, the theoretical trajectories are created in MATLAB for both experiments which provide the simulation time with respect to the maximum angular velocity of the motor after gear reduction. Followed by that the results of both experiments in vertical and horizontal orientations of the mechanism are presented.

Theoretical curves

Before performing the experiments, it is necessary to identify the simulation time required to attain the desired tilt position. The maximum angular velocity of the DC-Motor is around 0.25 rad/s after gear reduction. From the singularity analysis curves, at $2\pi/15$ radians, the spring attached to Motor-1 pulls the end-effector platform while at $-2\pi/15$ radians, Motor-2 and Motor-3 pulls the end-effector platform. Using the IKP relations, the other set of input tilt angles are found to be $[\eta, \phi]$ = [$\pm 7\pi/60$, $\pm\pi/15$] radians. The input tilt angles for performing both experiments are chosen within the singularity-free workspace square of the 3-SPS-U tensegrity mechanism. The trace of trajectory of input tilt angles chosen within the workspace of the mechanism is represented below in Fig. 3. The desired angular positions of the pulley for each steps of both experiments are calculated with the help of IKP and the pulley radius. The maximum angular position for the one spring pull is around ± 1.25 radians and for the two springs pull it is around ± 1.1 radians. Using Eqn. (9), for a maximum angular velocity of 0.25 rad/s motor after gear reduction and the norm being the maximum angular position of

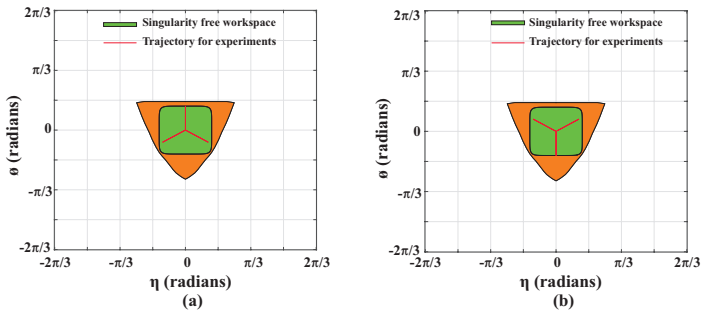

FIGURE 3. Trace of the desired input trajectories chosen for the (a) one spring pull and (b) two springs pull experiments within the workspace of the tensegrity mechanism

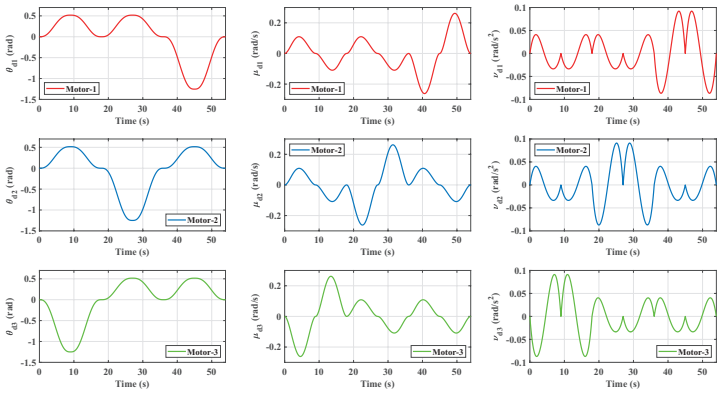

FIGURE 4. Theoretical angular positions (θ_d), velocities (μ_d) and accelerations (ν_d) of the pulleys of Motor-1 (red), Motor-2 (blue) and Motor-3 (green) for one spring pull experiment

the experiment, the simulation time to perform one cycle of the experiment is found to be 9 s for both experiments. Each experiment comprises of six steps and at the end, the mechanism is returned to the home position.

Thus, the total theoretical simulation time to perform the six steps is around 54 s. The theoretical curves are represented in Fig. 4 and Fig. 5. From the traces it is found that the maximum angular velocity of 0.25 rad/s is reached when the pulley travels between home position to ± 1.25 radians for one spring pull and ± 1.1 radians for two springs pull experiments.

Results of one spring pull experiment The one spring pull experiment is performed on the 3-SPS-U tensegrity mechanism for vertical and horizontal orientations. The simulation time for each cycle of the experiment is set at 9 s so that the maximum velocity is reached. The control algorithm consists of sleep routines between each cycle for smoother operations. Thus, the total time taken to perform the one spring pull experiments

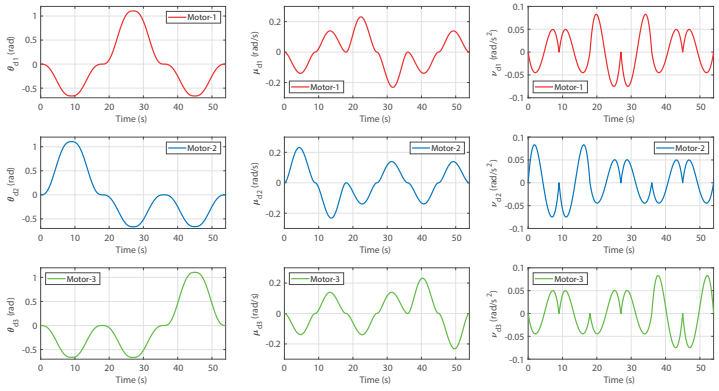

FIGURE 5. Theoretical angular positions (θ_d), velocities (μ_d) and accelerations (ν_d) of the pulleys of Motor-1 (red), Motor-2 (blue) and Motor-3 (green) for two springs pull experiment

is around 128 s. At each instance of the experiment, the IKP is calculated for the input tilt angles. The minimum length reached by one of the actuated prismatic spring is 43 mm while the other two springs reaches a maximum length of 78 mm. The plot of the joint positions (IKP) of each actuated prismatic joint from the experiment is represented below in Fig. 6 for both orientations of the mechanism. In Fig. 6, the dotted black line in each

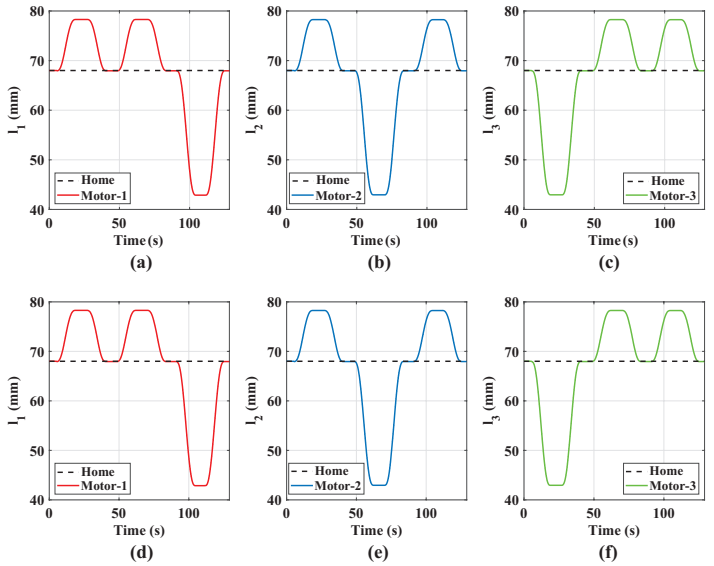

FIGURE 6. Position of prismatic springs along the linear trajectory for one spring pull experiment in the (a),(b),(c): vertical and (d),(e),(f): horizontal orientations of the mechanism

plot represents the home position of the mechanism at 68 mm. From the obtained results, the error can be calculated between

the measured and desired angular positions of the pulley using the equation:

$$Error = \frac{(\theta_{mi} - \theta_{di})180}{\pi} \tag{18}$$

Due to the frequency issues associated with the BB black microcomputer, higher noises were observed in the plots. In order to reduce these errors, the frequency of the results was measured in MATLAB and the Savitzky-Golay filtering method [23] was applied to reduce the noise. This filtering technique uses the least-squares method for smoothing signals without distorting it. The plot of error data for the one spring pull experiment after filtering is represented in Fig. 7. From Fig. 7, the global error between the desired and measured data lies between -0.03° to -0.05° for the cable pull and 0.04° to 0.05° for the cable push operations in both orientations of the mechanism. This also suggests that a simple PID control loop is sufficient for the tilting of the mechanism, provided the same motor units are employed. At each instance of the experiment, the torque induced on each motor to perform cable pull or push is also computed. The PID control algorithm returns the measured current and by using the torque constant, the torque induced on each motor is calculated. The representation of motor torques for both orientations after application of Savitzky-Golay filtering is shown in Fig. 8. The operating torque and the peak torques measured from experiments are found to be around one-third of the nominal motor torque. The torque values almost remains similar for both orientations of the mechanism. The maximum torque attained by one of the motor during cable pull is around -0.0015 N.m in both vertical and horizontal orientations. The effects of gravity and self-weight of the mechanism has negligible effects on the motors torques.

Results of two springs pull experiment Followed by the one spring pull, the two springs pull experiments are performed. Unlike the one spring pull, the length reached by two of the springs is around 54.8 mm over 43 mm while the third spring reaches a maximum length of 90 mm. As two springs operate to reach the desired tilt angle, the efforts are distributed among both motors to pull or push the end-effector platform. The total time taken to perform the two springs pull experiment is also 128 s, taking into account the sleep routines included in the control loop. The plot of the joint positions which provides the solutions to the IKP is represented in Fig. 9 for both orientations of the mechanism. The error between the desired and measured angular position of the pulley is calculated. The plots of error data for the two springs pull experiments for both orientations after application of numerical filtering are represented in Fig. 10. From Fig. 10, the global error between the measured and desired position data lies between -0.03° to -0.05° for the cable pull and 0.02° to 0.07° for cable pull and push operations in both orientations of the mechanism. Similar to the one spring pull experiments, good feedback could be observed from the PID control for the two spring pull experiments. However, a slight peak in error data could be observed in the vertical orientation. This issue arose due to the slight loosening of the cable or in other words, the tension in the cable was slightly less to hold the platform tightly. Using the current data from PID control loop, the torques on each motor are computed and their plots after application of numerical filtering are represented in Fig. 11. In the two springs pull experiment, the amount of torque required on two motors that pull the end-effector are comparatively lesser than the one spring pull experiment as the efforts are distributed among two motors. During the two springs pull experiment, a slight increase in motor torque could be observed for the horizontal orientation of the mechanism (0.002 N.m) over the vertical orientation (0.001 N.m) on Motor-2 for the first cycle. This is caused by the self-weight of the mechanism during horizontal orientation as the experimental setup behaves similar to a cantilever beam. However, these differences are not significant and can only be better interpreted with the additional of an external load on the mechanism.

DISCUSSIONS

The linear trajectory experiments were performed to understand if the mechanism could operate within the singularity-free workspace. The 3-SPS-U tensegrity mechanism was made to tilt up-to its maximum limit of $\pm 2\pi/15$ radians by conducting two types of experiments. In the first experiment, one of the three springs were pulled to the desired tilt limit whereas in the second experiment two springs were pulled to the desired tilt limit. In the case of one spring pull experiments, at the desired tilt position, the prismatic spring almost reached its maximum closed length. At this position, a slight movement of the fixed base was also observed and this was mainly caused by the material used for the base and end-effector of the mechanism. Rigid and lightweight metal such as aluminium can be replaced over ABS for the platforms such that the springs do not reach their minimum limits and the movements of the platform could be arrested. From the experiments, the mechanisms were able to operate smoothly and no singular configurations were reached as the input tilt limits were chosen at the boundaries of the singularity-free workspace square. The error data obtained from both experiments also proved the effectiveness of the PID control algorithm. From the experiments, it was possible to identify the motor torques required for actuation of the mechanism during each cycle. Since a lightweight material was employed for the mechanism, the effects of gravity and self-weight had limited contributions to the motor torques for horizontal orientation. Thus, similar results were observed for both orientations of the mechanism. At each instance of the experiments, it is also possible to compute the desired input angles and using the IKP, the actual solutions to the

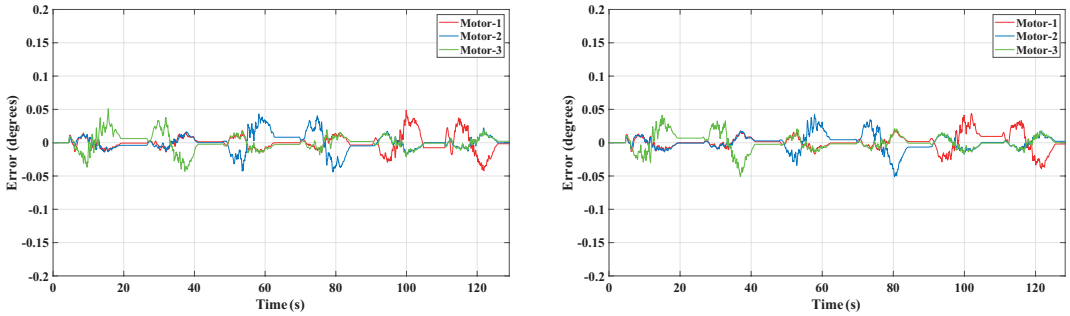

FIGURE 7. Joint position errors along the linear trajectory in the (a) vertical and (b) horizontal orientations of the mechanism for the one spring pull experiment

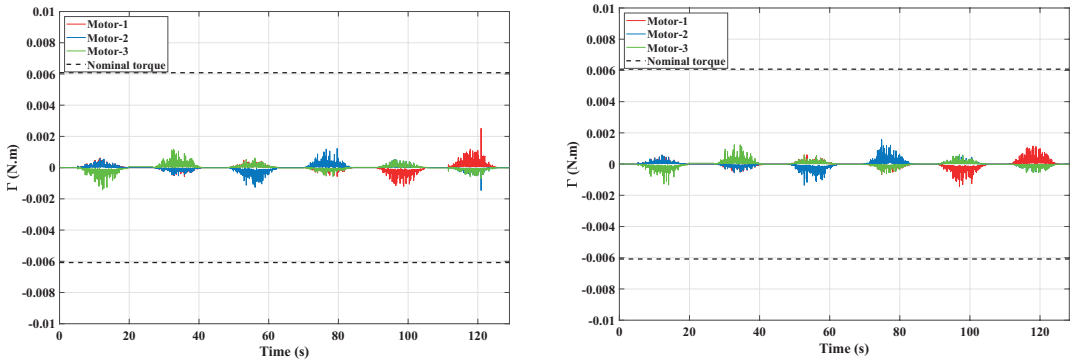

FIGURE 8. Motor torques during operation along the linear trajectory in the (a) vertical and (b) horizontal orientations of the mechanism for the one spring pull experiment

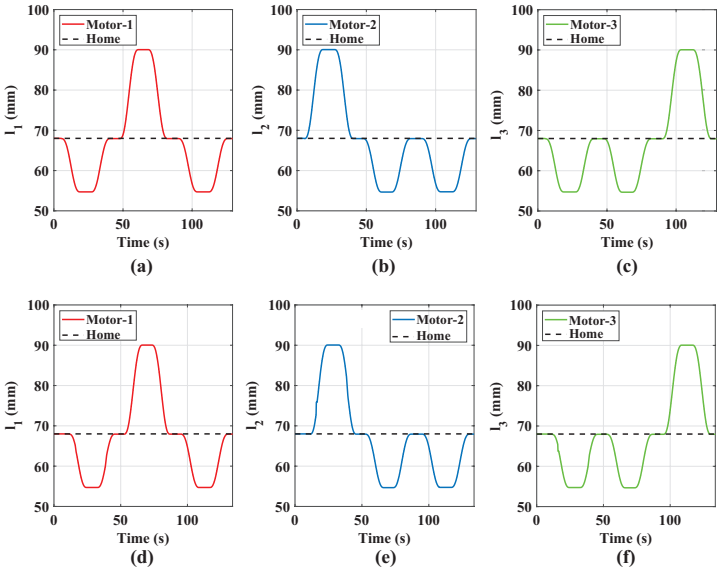

FIGURE 9. Position of prismatic springs along the linear trajectory for two springs pull experiment in the (a),(b),(c): vertical and (d),(e),(f): horizontal orientations of the mechanism

DKP can be determined. However, this process is computationally expensive to carry out in C or MATLAB for the entire experimental cycle. When comparing both experiments, the prismatic retraction along one of the spring was higher for the one spring pull when compared to the two springs pull experiment. This comparison is shown in Fig. 12. At a particular orientation of the tensegrity mechanism at the home-pose as shown in Fig. 12b, the position of one of the prismatic links is located at a distance of r_f while the other prismatic links are located at a distance of $r_f/2$ from the central axis. By the lever arm principle, during the one spring pull experiment, the prismatic link has to retract to a longer length (Fig. 12a) when compared to the two springs pull (Fig. 12c) experiment for attaining the desired input tilt angles. However, it has to be noted that the combined operating torques of all the motors remains the same for both experiments. The video link for the linear trajectory experiments is provided at the bottom of this page [1] .

[1] Video link for the linear trajectory experiments: `https://uncloud.univ-nantes.fr/index.php/s/jfyj7qE2NRZ9exS`

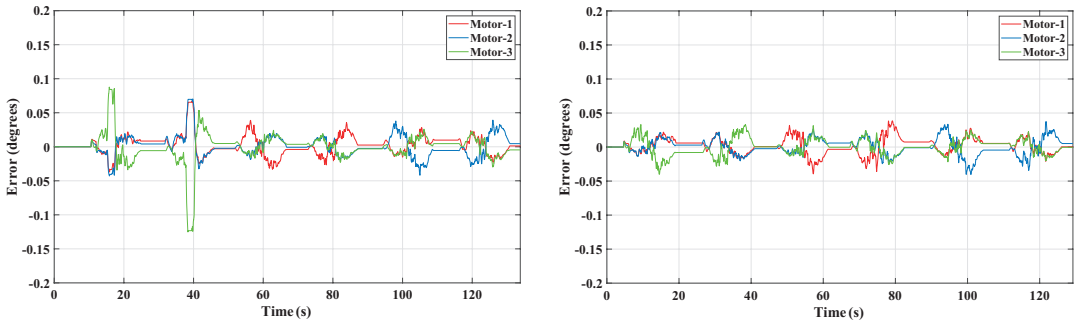

FIGURE 10. Joint position errors along the linear trajectory in the (a) vertical and (b) horizontal orientations of the mechanism for the two springs pull experiment

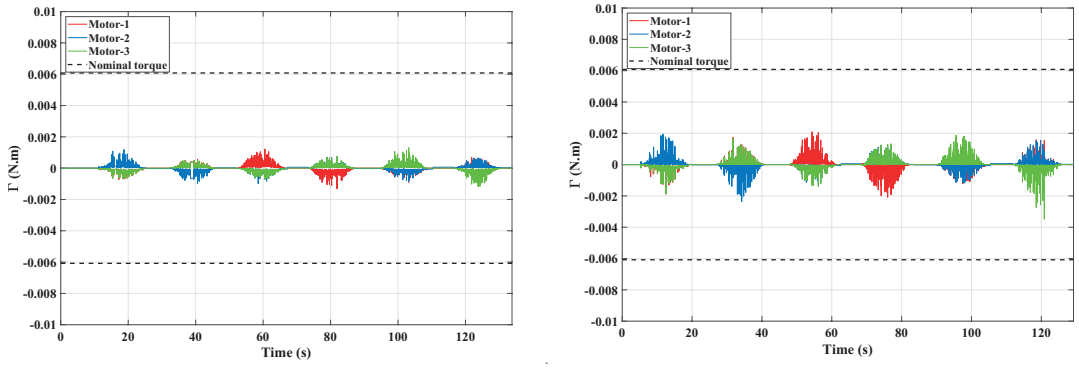

FIGURE 11. Motor torques under operation along the linear trajectory in the (a) vertical and (b) horizontal orientations of the mechanism for the two springs pull experiment

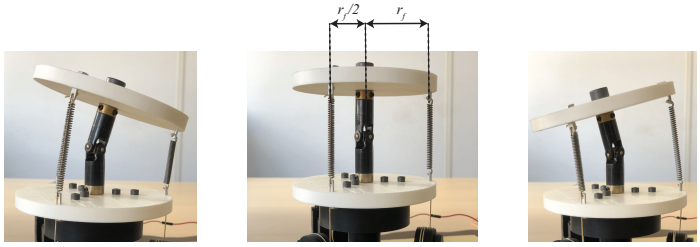

FIGURE 12. Postures of the tensegrity mechanism during (a) One spring pull, (b) Home-pose and (c) Two springs pull phases of the experiments

CONCLUSIONS

This article presented the experimental validation on the prototype of a 3-SPS-U tensegrity mechanism. Using DC-motors coupled with geartrain and servo controllers, the actuation of the springs of the mechanism was carried out. Through a force control algorithm written in C language, a simple closed-loop PID control was created to tilt the tensegrity mechanism. A linear trajectory was studied and validated experimentally in vertical and horizontal orientations of the mechanism for given input tilt angles. The IKP for the tensegrity mechanism was solved experimentally through the Jacobian matrix and its time derivatives, which appeared simpler. Two sets of experiments were conducted. In the first type, one of the three motors connected to the spring was actuated to tilt the end-effector along a given linear path, whereas in the second type two of the three motors were actuated to pull the end-effector platform. Theoretical plots for positions, velocities and accelerations were presented for identifying the simulation time required with respect to the maximum velocity of motors after gear reduction. Experiments were then carried out on the prototype developed at LS2N. After each tilt operation, the mechanism was made to return to the home-pose. This was mainly performed to understand the accuracy of the PID control loop. The error between measured and desired data were lower than 0.05° for most trajectories and it proved the effectiveness of the PID controller. With the horizontal orientation of the mechanism, there were no significant differences observed in the motor torques. However, this parameter will not appear the same when the mechanism is coupled along with the rigid bio-inspired robot. It was also found that the mechanism did not attain singular configurations during the experiments as the input tilt angles were chosen at the boundaries of the singularity-free workspace. However, the prismatic springs reached their min-

imum closed length during the one spring pull experiments as slight movements were observed on the fixed base of the tensegrity mechanism.

At present, experiments under the presence of an external load are being carried out to understand the differences in motor torques for the two orientations of the mechanism. In the future works, a circular trajectory experiment will be carried out which will have correlation with the Tilt & Torsion theory. This trajectory can be useful for the mechanism when coupled along with the rigid piping inspection robot as this trajectory can help align the axis of the robot along the axis of the pipeline for real time applications. Also, in the future works, an EtherCAT based controller will be incorporated to operate the tensegrity mechanism and the modules of the piping inspection robot from a central platform.

REFERENCES

[1] Skelton, R. E., Adhikari, R., Pinaud, J.-P., Chan, W., and Helton, J., 2001. "An introduction to the mechanics of tensegrity structures". In Proceedings of the 40th IEEE conference on decision and control (Cat. No. 01CH37228), Vol. 5, IEEE, pp. 4254–4259.

[2] Arsenault, M., and Gosselin, C. M., 2006. "Kinematic, static and dynamic analysis of a planar 2-dof tensegrity mechanism". *Mechanism and Machine Theory,* ***41***(9), pp. 1072–1089.

[3] Crane, C. D., Bayat, J., Vikas, V., and Roberts, R., 2008. "Kinematic analysis of a planar tensegrity mechanism with pre-stressed springs". In *Advances in Robot Kinematics: analysis and design*. Springer, pp. 419–427.

[4] Bakker, D. L., Matsuura, D., Takeda, Y., and Herder, J. L., 2015. "Design of an environmentally interactive continuum manipulator". In Proc. 14th World Congress in Mechanism and Machine Science, IFToMM.

[5] Tantaworrasilp, A., and Richardson, R. C., 2020. "Metamorphic tensegrity structure for pipe inspection". In IOP Conference Series: Materials Science and Engineering, Vol. 715, IOP Publishing, p. 012087.

[6] Wenger, P., and Chablat, D., 2018. "Kinetostatic analysis and solution classification of a planar tensegrity mechanism". In *Computational Kinematics*. Springer, pp. 422–431.

[7] Snelson, K. D., 1965. Continuous tension, discontinuous compression structures, Feb. 16. US Patent 3,169,611.

[8] Chen, S., and Arsenault, M., 2012. "Analytical computation of the actuator and cartesian workspace boundaries for a planar 2-degree-of-freedom translational tensegrity mechanism". *Journal of Mechanisms and Robotics,* ***4***(1).

[9] Venkateswaran, S., Chablat, D., and Boyer, F., 2019. "Numerical and experimental validation of the prototype of a bio-inspired piping inspection robot". *Robotics,* ***8***(2), p. 32.

[10] Venkateswaran, S., Furet, M., Chablat, D., and Wenger, P., 2019. "Design and analysis of a tensegrity mechanism for a bio-inspired robot". In Proceedings of the ASME 2019 IDETC-CIE, Vol. 5A: 43rd Mechanisms and Robotics Conference. V05AT07A026.

[11] Merlet, J.-P., 2005. *Parallel robots*, Vol. 128. Springer Science & Business Media.

[12] Venkateswaran, S., Chablat, D., and Ramachandran, R., 2019. "Prototyping a piping inspection robot using a beaglebone black board". In 24ème Congrès Français de Mécanique.

[13] Gosselin, C., and Angeles, J., 1990. "Singularity analysis of closed-loop kinematic chains". *IEEE transactions on robotics and automation,* ***6***(3), pp. 281–290.

[14] Wenger, P., and Chablat, D., 1997. "Definition sets for the direct kinematics of parallel manipulators". In 1997 8th International Conference on Advanced Robotics. Proceedings. ICAR'97, IEEE, pp. 859–864.

[15] Chablat, D., and Wenger, P., 1998. "Working modes and aspects in fully parallel manipulators". In Proceedings. 1998 IEEE International Conference on Robotics and Automation (Cat. No. 98CH36146), Vol. 3, IEEE, pp. 1964–1969.

[16] Venkateswaran, S., and Chablat, D., 2020. "Singularity and workspace analysis of 3-sps-u and 4-sps-u tensegrity mechanisms". In International Symposium on Advances in Robot Kinematics, Springer, pp. 226–233.

[17] Venkateswaran, S., Chablat, D., and Hamon, P., 2021. "An optimal design of a flexible piping inspection robot". *Journal of Mechanisms and Robotics,* ***13***(3), p. 035002.

[18] Maung, M. M., Latt, M. M., and Nwe, C. M., 2018. "Dc motor angular position control using pid controller with friction compensation". *International Journal of Scientific and Research Publications,* ***8***(11), p. 149.

[19] Maxon motors,program 2017/18. high precision drives and systems. `http://epaper.maxonmotor.com/`. Accessed: 2017-12-15.

[20] Khalil, W., and Dombre, E., 2004. *Modeling, identification and control of robots*. Butterworth-Heinemann.

[21] Caro, S., Chablat, D., Lemoine, P., and Wenger, P., 2015. "Kinematic analysis and trajectory planning of the orthoglide 5-axis". In Proceedings of the ASME 2015 IDETC-CIE, Vol. 5C: 39th Mechanisms and Robotics Conference. V05CT08A004.

[22] Jha, R., Chablat, D., Rouillier, F., and Moroz, G., 2016. "Influence of the trajectory planning on the accuracy of the orthoglide 5-axis". In Proceedings of the ASME 2016 IDETC-CIE, Vol. 5A: 40th Mechanisms and Robotics Conference. V05AT07A039.

[23] Savitzky-golay filtering. `https://fr.mathworks.com/help/signal/ref/sgolayfilt.html/`. Accessed: 2020-08-28.